Spectroelectrochemical Characterization of Small Hemoproteins Adsorbed within Nanostructured Mesoporous ITO Electrodes

Delphine Schaming, Christophe Renault, Ryan Tucker, Stéphanie Lau-Truong, Jean Aubard, Michael Brett, Véronique Balland, Benoît Limoges

Spectroelectrochemical Characterization of Small Hemoproteins Adsorbed within Nanostructured Mesoporous ITO Electrodes

Delphine Schaming,[†] Christophe Renault,[†] Ryan T. Tucker,[‡] Stéphanie Lau-Truong,[£] Jean Aubard,[£] Michael J. Brett,[‡,xx] Véronique Balland*[,†] and Benoît Limoges*[,†]

[†] Laboratoire d'Electrochimie Moléculaire, UMR CNRS 7591, Université Paris Diderot, Sorbonne Paris Cité, 15 rue Jean-Antoine de Baïf, F-75205 Paris Cedex 13, France

[‡] Electrical and Computer Engineering, University of Alberta, Edmonton, Alberta, Canada T6G 2V4

[£] Laboratoire ITODYS, UMR CNRS 7086, Université Paris Diderot, Sorbonne Paris Cité, 15 rue Jean-Antoine de Baïf, F-75205 Paris Cedex 13, France

[xx] NRC National Institute for Nanotechnology, Edmonton, Alberta, Canada T6G 2M9

KEYWORDS. protein-film voltammetry • cyclic voltabsorptometry • spectroelectrochemistry • mesoporous film • indium tin oxide

Supporting Information Placeholder

ABSTRACT: 3D nanostructured transparent indium tin oxide (ITO) electrodes prepared by glancing angle deposition (GLAD) were used for the spectroelectrochemical characterization of cytochrome c (Cyt c) and neuroglobin (Nb). These small hemoproteins, involved as electron-transfer partners in the prevention of apoptosis, are oppositely charged at physiological pH and can each be adsorbed within the ITO network under different pH conditions. The resulting modified electrodes were investigated by UV-visible absorption spectroscopy coupled with cyclic voltammetry. By using non-denaturating adsorption conditions, we demonstrate that both proteins are capable of direct electron transfer to the conductive ITO surface, sharing apparent standard potentials similar to those reported in solution. Preservation of the 3D protein structure upon adsorption was confirmed by resonance Raman (rR) spectroscopy. Analysis of the derivative cyclic voltabsorptograms (DCVA) monitored either in the Soret or the Q bands at scan rates up to 1 V s^{-1} allowed us to investigate direct interfacial electron transfer kinetics. From the DCVA shape and scan rate dependences, we conclude that the interaction of Cyt c with the ITO surface is more specific than Nb, suggesting an oriented adsorption of Cyt c and a random adsorption of Nb on the ITO surface. At the same time, Cyt c appears more sensitive to the experimental adsorption conditions and complete denaturation of Cyt c may occur as evidenced from cross-correlation of rR spectroscopy and spectroelectrochemistry.

INTRODUCTION

Direct electron transfer protein-film spectroelectrochemistry is a powerful emerging method for analyzing the electron transfer processes in immobilized redox proteins or enzymes.[1] It is based on the monitoring of the spectroscopic features of a (sub-)monolayer redox protein in a coupled electrochemical experiment, leading to key information on the structural integrity of the immobilized protein, allowing unambiguous attribution of the redox potentials of the different species and intermediates, and depending on the spectroscopic method used, assisting in the determination of the electroactive surface coverage (which often lies below the detection limit in cyclic voltammetry). Moreover, when significant time-resolution can be achieved, it offers the possibility of better insights into the interfacial electron transfer kinetics and the link to coupled chemical reactions.[2, 3] It is therefore particularly relevant in fundamental studies of long-range electron transfers, enzyme reactivities and mechanisms, and also for applications requiring immobilized biomolecules such as in electrochemical biosensors, biofuel cells and bioreactors.[4, 5]

The main difficulty encountered with the development of protein-film spectroelectrochemistry is the spectroscopic detection of low protein coverage (~ pmol cm^{-2}) with satisfactory signal-to-noise ratio. This is especially emphasized when short integration times are required to achieve significant time-resolution. Single-scan detection of protein (sub-)monolayers can be achieved by optical spectroscopies with either a highly sensitive technique such as fluorescence[6] or with absorbance spectroscopy by increasing the optical path length or electrode surface.[7, 8] Both approaches have been coupled with cyclic voltammetry in real-time spectroelectrochemical experiments.[3, 9] One major advantage of this methodology is that the spectroscopic signal is free of the capacitive contribution from the electrode. Moreover, multicomponent analysis can be performed by simultaneously monitoring a selection of wavelengths using diode-array or CCD detectors. This methodology was successfully used to unambiguously attribute redox potentials in a multiheme protein[10] and to analyze the heterogeneous electron transfer rates of immobilized biomolecules such as flavodoxin,[8] microperoxidase-11 (MP-11)[11] or azurin.[6] More recently, we have demonstrated that cross-correlation of the

spectroscopic and electrochemical data obtained by real-time spectroelectrochemistry allows mechanistic investigation and quantitative kinetic analysis of the redox-linked catalytic activity of an immobilized biomolecule.[12]

In the particular case of UV-visible absorption spectroelectrochemistry of a protein sub-monolayer, satisfactory signal-to-noise ratio can be achieved with the use of transparent electrode with high surface area. This has been illustrated with thin films of mesoporous metal oxides made of randomly sintered nanoparticles of SnO_2 or TiO_2.[8, 10, 13] However, because of their semi-conductive properties, the accessible potential window and scan rate range are greatly limited. Improvement of the electronic conductivity of these metal oxide films can be achieved by addition of an extrinsic dopant leading to materials such as ITO (indium tin oxide) or ATO (antimony tin oxide). Only a few methods are suitable to fabricate mesoporous doped metal-oxide films with a large surface area and an open, accessible porosity. Among them, the vacuum-based glancing angle deposition (GLAD) technique is a single-step physical method which allows the fabrication of mesoporous ITO films with a high degree of control in film porosity and thickness.[14,15] The resulting conductive ITO films are typically made of nanosized columnar structures with a relatively well-defined nanoporosity and thicknesses up to few micrometers.[16] We have recently shown that these well-defined porous films of high surface area can be useful for the real-time spectroelectrochemical characterization of the MP-11 reactivity towards dioxygen.[11, 12]

In the present paper, we explore the potential offered by mesoporous GLAD ITO electrodes for the adsorption and spectroelectrochemical characterization of larger hemoproteins. The first one is cytochrome c (Cyt c), a hemoprotein of 12.4 kDa, well-known to undergo direct electron transfer with different electrode surfaces, including ITO.[17-19] It is characterized by an isoelectric point (pI) of 10-10.5 and a positively charged lysine patch that governs orientation of the protein on negatively charged surfaces.[20] The second one is the neuroglobin (Nb), a hemoprotein with a similar size to Cyt c (MW of 17 kDa) but with an opposite isoelectric point of 5.4.[21, 22] Similar to Cyt c, Nb was shown to undergo direct electron transfer when immobilized on a metal electrode.[23] The exact role of Nb is not yet known. It has however been suggested that Nb may reduce Cyt c in the interception of the initial steps of apoptosis, with formation of an intermediate complex involving electrostatic interactions.[24, 25] We demonstrate here, by UV-visible absorption and resonance Raman (rR) spectroscopy, that both proteins can be efficiently adsorbed in the three-dimensional ITO network. In the case of Cyt c, structural change may occur depending on the experimental conditions. Moreover, once adsorbed, both proteins are able to directly exchange an electron with the conductive ITO surface. The thermodynamic and kinetic parameters of the heterogeneous electron transfer were examined in detail by UV-visible absorption spectroelectrochemistry, leading to the conclusion that Nb adsorbs in a random orientation towards the ITO surface whereas Cyt c is most likely oriented.

RESULTS AND DISCUSSION

Electrode functionalization. 2-μm-thick GLAD ITO electrodes were prepared as described elsewhere by using a deposition angle of 80°.[16] The films are made of nanosized columnar structures of ITO deposited onto a commercial flat ITO substrate (Figure 1 shows witness sample prepared on a Si substrate). The film porosity is ca. 0.5. On the top of the 2-μm ITO film, the void spacing between the columns is ca. 90 nm and it decreases with the depth in the film,[26] whereas the column density increases. It was previously shown that the electroactive surface area increases linearly with the film thickness and that the electroactive surface area enhancement is ca. 130 for a 2-μm GLAD ITO film.[12]

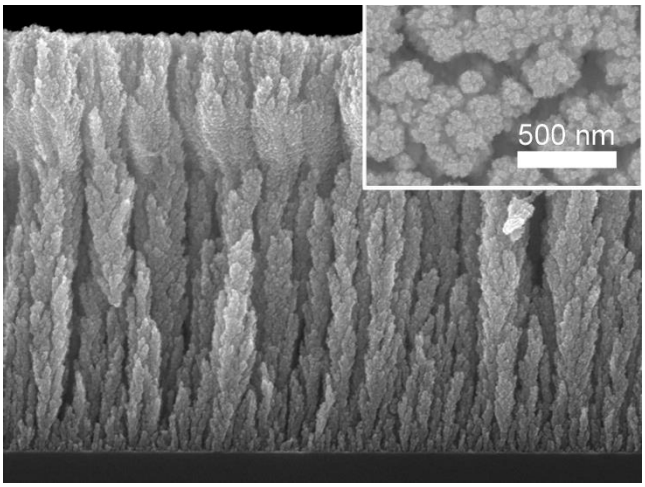

Figure 1. SEM images (side- and (Inset) top-views) of a 2-μm GLAD ITO film prepared with a deposition angle of 80°.

The hemoproteins were incorporated in the GLAD ITO films by passive adsorption. The ITO electrodes were immersed in an appropriate low ionic strength buffer solution containing sub-micromolar concentration of the protein. These conditions are favorable to a binding by electrostatic interaction between the hemoprotein and the ITO surface. Although the isoelectric point of the GLAD ITO films is not precisely known, it is thought to lie between 6.0, the experimental value obtained for ITO nanoparticles dispersed in water,[27] and 8.5, the theoretical value calculated for In_2O_3 nanoparticles containing 10% SnO_2.[28] As it will be discussed later on, prior to protein adsorption, the GLAD ITO electrodes were preconditioned in a protein-free buffer solution for at least 12 hours to avoid significant protein denaturation, especially in the case of Cyt c.

After an adsorption time ranging from a few minutes to several hours, the amount of protein adsorbed in the transparent ITO film was determined by UV-visible absorption spectroscopy in a protein-free buffer. The adsorption of Cyt c within the mesoporous ITO electrodes was observed to be efficient and relatively fast at pH 7.0 in a 10 mM Hepes buffer solution. At this pH, Cyt c is positively charged and it is likely that adsorption is mainly driven by electrostatic interaction with the negatively charged ITO surface, similar to reports of other metal oxides such as TiO_2.[13, 29] Equilibrium is almost reached after 1 hour adsorption time in the presence of 50 μM Cyt c in solution (Figure S1 in Supporting Information). A typical UV-visible absorption spectrum of a Cyt c-ITO electrode is shown in Figure 2A.

Under same experimental conditions (*i.e.* 10 mM Hepes buffer of pH 7.0) adsorption of Nb was observed to be inefficient

since no protein could be detected by UV-visible absorption spectroscopy within the ITO film after 1 hour adsorption time. At pH 7.0, Nb (pI = 5.4) is negatively charged and behaves oppositely to the positively charged Cyt c. This confirms that protein adsorption is mainly driven by electrostatic interactions and that the isoelectric point of the GLAD ITO film lies most likely below 7.0. However, upon slight acidification of the solution at pH 5.5 (10 mM MES Buffer), efficient adsorption of Nb was observed. At this pH, Nb is still slightly negatively charged and the ITO surface most likely positively charged.[27] Under this experimental condition, equilibration of the ITO electrode was almost reached within 1 hour immersion time in a 50 µM Nb solution. The corresponding UV-visible spectrum is given in Figure 2C. A similar effect of pH on protein adsorption was reported for azurin (pI~5.6) adsorbed in mesoporous ATO electrodes.[30]

The adsorption kinetic plots of Cyt c monitored by UV-visible absorption spectroscopy were fit to a double exponential function assuming a pseudo first-order kinetic (Figure S1). This double exponential fit suggests that a fast primary fraction of Cyt c adsorbs rapidly (k_1 = 0.4 min^{-1}) followed by a secondary fraction which leads to complete saturation of the film within a few hours (k_2 = 0.015 min^{-1}). The kinetic rate values are very close to the one reported for the adsorption of MP-11 in GLAD ITO electrodes under the same experimental conditions (*ie.* 50 µM MP-11, 10 mM Hepes, pH 7.0).[12] The stability of the resulting Cyt c-ITO electrode was characterized in the buffer solution used for the spectroelectrochemical experiments (90 mM Hepes, 10 mM NaCl) and, after 30 minutes, only a small fraction (ca. 15 %) of Cyt c was observed to desorbs whereas the remaining fraction was strongly retained over a few hours, allowing a series of spectroelectrochemical experiments to be performed with the same protein-loaded electrode and minimal change in the protein-film concentration. Similar results were obtained for Nb-ITO electrodes in MES buffer at pH 5.5. It has to be mentioned that the desorption process is highly sensitive on the buffer ionic strength and that increasing of the buffer ionic strength leads to fast and efficient desorption of the adsorbed proteins. This confirms that electrostatic interactions are involved in the adsorption process.

Spectroscopic characterization. It can be clearly seen in the UV-visible absorption spectra of the modified electrodes that the Soret bands of adsorbed proteins overlap with the intense band-to-band absorbance of the ITO film that exponentially grows in the UV region as the wavelength decreases. The absorbance spectrum of the protein-free ITO electrode was thus subtracted from the spectra of the protein-loaded GLAD ITO electrodes (Figure 2). On the resulting corrected spectra, the maximum wavelength of the Soret band lies at 407 nm for Cyt c and 412 nm for Nb, which is similar to that obtained for the proteins diluted in solution. This result suggests that the UV-visible spectroscopic characteristics of both proteins are not significantly affected by their adsorption within the transparent mesoporous structure. However, as it can be discerned in Figure 2B and 2D, the blank subtracted spectra of Cyt c and Nb is far from ideal since a large residual band-to-band absorbance of the ITO film remains. This problem of imperfect blank correction was attributed to a systematic red-shift of the band-to-band UV absorbance to larger wavelengths. This likely result from interfacial modification of the electronic properties of GLAD ITO films upon protein adsorption.

To obtain more information about the heme environment and, to some extent, on the structural conformation of the adsorbed proteins, we have characterized the protein-loaded films by rR spectroscopy. The rR spectra were obtained at 405 nm laser excitation with a good signal-to-noise ratio over a large wavelength number range. These spectra are shown in Figure 2E and compared to the spectra recorded for the proteins diluted in solution. All spectra exhibit characteristic Raman bands of heme and no contribution of the underlying GLAD ITO electrode. The coordination/spin state-sensitive ν_2 (1591, 1582 cm^{-1}) and ν_3 (1503, 1505 cm^{-1}) bands and the redox state ν_4 marker band (1371, 1374 cm^{-1}) are typical of heme iron in an oxidized six-coordinated (6-c) low-spin (LS) state.[31] For both adsorbed proteins, the rR spectra a show high level of similarity with those recorded in solution. This confirms that no major structural change of the heme pocket of Cyt c and Nb occurs upon their adsorption in the ITO electrodes.

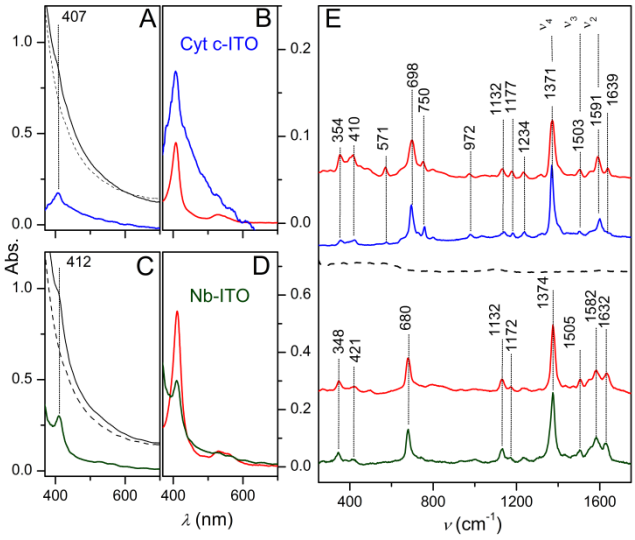

Figure 2. UV-visible absorption spectra of (—) Cyt c-ITO electrodes and (—) Nb-ITO electrodes (2-µm-thick films): (A, C) (—) raw spectrum, (-----) protein-free ITO spectrum, (—, —) blank-corrected spectrum. (B, D) Comparison between (—, —) the UV-visible spectra of adsorbed proteins with (—) those of proteins in a homogenous solution: (B) 10 µM Cyt c in a 1-mm path length cell and (D) 4.6 µM Nb in a 1-cm path length cell. (E) Resonance Raman spectra obtained under Soret excitation at λ_{exc} = 405 nm for respectively Cyt c and Nb, in solution (—) or adsorbed in the GLAD ITO electrodes (—, —). (-----) rR spectrum of a protein-free ITO electrode recorded under the same experimental conditions. All of the Cyt c spectra were recorded in a 10 mM Hepes buffer at pH 7.0, while all Nb spectra were performed in a 10 mM MES buffer at pH 5.5 (T = 20 °C).

Cyclic voltammetry and voltabsorptometry. The Cyt c-ITO and Nb-ITO electrodes were studied in cyclic voltammetry by simultaneously monitoring the absorbance variations at the Soret and Q-band wavelengths. Experiments were conducted at various scan rates, ranging from 0.005 to 1 V s^{-1}, and within the potential window corresponding to the reduction of Fe^{III}

into Fe^{II}. Satisfactory absorbance variation signal-to-noise ratios could be reached using integration times as low as 20 ms. Typical cyclic voltabsorptograms (CVAs) obtained at low scan rate are reported in Figure 3A. Both electrodes exhibit a well-defined reversible redox transition (Fe^{III}/Fe^{II} redox couple) centered at +0.26 V for Cyt c and -0.10 V for Nb. Identical apparent standard potential values ($E°'$) were obtained from spectroelectrochemical redox titration of the immobilized proteins (Figure S2). These $E°'$ values are in perfect agreement with the ones determined in homogeneous solution at pH 7.0, *ie.* +0.26 V for Cyt c and -0.10 V for Nb.[17, 23] The apparent standard potential of the Fe^{III}/Fe^{II} redox couples thus appears almost unaffected by the interaction with the ITO surface.

The amount of electroactive hemoproteins adsorbed in the GLAD ITO film (Figure S3) was calculated from the difference absorbance spectra obtained between the fully reduced and fully oxidized protein-loaded ITO electrode and by using the difference extinction coefficient values determined in homogenous solution. For Nb, a value of $\Gamma_{elec} = (6 \pm 1) \times 10^{-10}$ mol cm^{-2} was found (i.e., estimated in mol per unit of projected area of GLAD ITO film from the absorbance changes at either 424, i.e. $\Delta\varepsilon_{424} = \varepsilon^{FeII}-\varepsilon^{FeIII}$ = 135 000 M^{-1} cm^{-1}, or 558 nm, i.e. $\Delta\varepsilon_{558}$ = 23 500 M^{-1} cm^{-1}) which is fully consistent with the amount indirectly determined from integration of the faradaic peak current recorded in cyclic voltammety, i.e. 6.2 × 10^{-10} mol cm^{-2}. This is however much lower than the amount of Nb determined from the absolute Soret absorbance at 412 nm (corresponding to the native oxidized form of Nb, ε_{412} = *129 000* M^{-1} cm^{-1}), i.e. Γ_{Soret} = 21 10^{-10} mol cm^{-2}. The same divergence was observed for Cyt c since the electroactive amount deduced from the absorbance spectra difference (i.e., Γ_{elec} = 4.5 ± 1 10^{-10} mol cm^{-2}) was observed to be approximately 5 times lower than the amount of Cyt c calculated from the absolute Soret band absorbance of the oxidized species at 407 nm (ε_{407} = *106 000* M^{-1} cm^{-1}), Γ_{Soret} = 27 10^{-10} mol cm^{-2}. This large inconsistency between surface concentrations determined from difference absorbance spectra and absolute absorbance values may arise either from (i) a large fraction of electro-inactive proteins which cannot productively exchange electrons with the porous ITO network or, as it has been previously discussed, (ii) from a substantial absorbance contribution of the GLAD ITO film that cannot be appropriately corrected by blank subtraction. On the basis of the narrow Soret band obtained for both the reduced form of absorbed Cyt c and Nb we have concluded that nearly all of the adsorbed proteins can directly communicate and reversibly exchange their electron with the conductive ITO film. We are convinced that a systematic undercorrection of the UV-visible spectra of adsorbed proteins occur as evidenced by the obvious remaining contribution of the GLAD ITO absorbance in the subtracted spectra (Figures S4 and S5). Accordingly, we will use the values of Γ_{elec} in estimating surface coverage.

Surface concentrations of 0.45 and 0.60 nmol cm^{-2} that were finally estimated for both hemoproteins were equivalent to *ca.* 20 and 30 saturated monolayers on planar surfaces (i.e., considering a theoretical maximal surface coverage of γ^{sat} = 22 pmol cm^{-2} and 19 pmol cm^{-2} for Cyt c and Nb, respectively[23]). According to the estimated surface area enhancement of 130 for the 2-µm GLAD ITO electrode,[12] the Cyt c and Nb surface concentrations correspond to a surface coverage of 15 and 23%, respectively. For Cyt c, the value is lower than the one reported for adsorption on planar ITO electrodes, leading to a maximum surface coverage of 64% after one hour adsorption in a 20 µM protein solution (Table 1).[18] It is also much lower than the values reported for Cyt c adsorption within highly ordered mesoporous films of TiO_2 obtained under similar experimental conditions.[13] This low surface coverage might result from an inaccessible nanoporosity of the GLAD ITO network to the hemoproteins studied.[26] Higher surface coverages might probably be obtained by increasing either the protein concentration in the adsorption solution or the adsorption time, but as the adsorbed proteins could be easily detected by spectroscopy under our experimental conditions, we did not try to maximize the amount of protein adsorbed within the network.

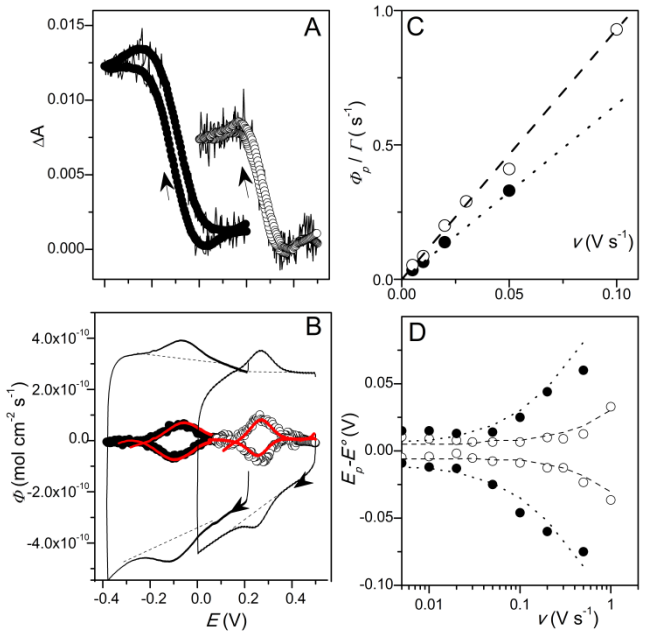

Figure 3. (A) Cyclic voltabsorptograms monitored at 556 and 548 nm at a (●) Nb-ITO and (○) Cyt c-ITO electrode (2-µm-thick) and (B) their corresponding simultaneously recorded CVs shown before (—) and after (—) subtraction of the background capacitive current. In B, the DCVAs (represented in flux density) of (●) Nb-ITO and (○) Cyt c-ITO electrodes are also reported. Scan rate: 20 mV s^{-1}. (C) DCVA peak current flux densities as a function of scan rate for: (●) Nb-ITO and (○) Cyt c-ITO electrodes. Dashed lines: linear fits with slopes of 6.6 and 9.2 V^{-1}, respectively. (D) Trumpet plots obtained from the anodic and cathodic peak potentials in DCVAs as a function of scan rate: (●) Nb and (○) Cyt c. The dashed curves are the Butler-Volmer theoretical fits using for Nb k_s = 2 s^{-1} and α = 0.5, and for Cyt c k_s = 12 s^{-1} and α = 0.5. All experiments were done in a 90 mM Hepes, 10 mM NaCl, pH 7.0 for Cyt c and in a 10 mM MES, 10 mM NaCl at pH 5.5 for Nb. T = 20°C.

The derivative cyclic voltabsorptograms (DCVAs) obtained after time derivation of CVAs are equivalent to cyclic voltammograms (CVs) when both are expressed in flux density Φ according to the following equation:

$$\phi = -\frac{1}{\Delta\varepsilon_\lambda}\frac{dA_\lambda}{dt} = \frac{i}{nFS} \quad (1)$$

Where A_λ is the absorbance at the wavelength λ, $\Delta\varepsilon_\lambda$ the difference in the extinction coefficients between the reduced and oxidized species expressed in $mol^{-1}cm^2$, n the theoretical number of electrons involved in the redox reaction (n = 1 for the Fe^{III}/Fe^{II} redox couple), F the Faraday constant (96500 C mol^{-1}), and S the geometric electrode surface area.

In Figure 3B, the simultaneously recorded DCVAs and CVs are reported for both Cyt c- and Nb-ITO electrodes. Intensities of the reversible DCVA waves were almost identical to the ones obtained with background-subtracted CVs (*i.e.,* CVs subtracted from their large background capacitive current). As expected for surface-confined electroactive centers, anodic and cathodic peak current flux densities show linear dependencies with the scan rate (Figure 3C). From linear regressions to the experimental data, slope values of 9.2 and 6.6 V^{-1} were obtained for Cyt c and Nb, respectively. The latter significantly differs from the value of 9.9 V^{-1} expected for an ideal one-electron Nernstian redox couple at 20 °C. It is also clear from the CVA that the redox transition occurs more abruptly for Cyt c than Nb. As a result, the full width at half maximum (fwhm) of the cathodic and anodic peaks in the DCVA of Nb is larger (160 mV) than the one reported for Cyt c (120 mV), even though both data differ noticeably from the theoretical fwhm value of 89 mV for a reversible one-electron electron transfer at 20 °C. Regardless, the experimental data for Cyt c are much closer to those expected for an ideal Nernstian redox couple, suggesting a relatively homogeneous and well-defined environment around the heme redox center from the thermodynamic point of view. This probably results from a more specifically oriented adsorption of Cyt c on the ITO surface than for Nb. Indeed for Nb, the higher deviation from an ideal Nernstian behavior can be attributed to a random orientation of absorbed Nb on the ITO surface, leading to a distribution of microenvironments around the heme center and thus a distribution of standard potentials.[32] This can be modeled by an apparent value, n_{app}, that deviates from the theoretical value of n = 1 for a Fe^{III}/Fe^{II} redox couple.[23] From the experimental data, n_{app} values of 0.6 and 0.85 were obtained for Nb and Cyt c, respectively.

With the aim to evaluate the heterogeneous electron transfer rate for each hemoprotein, the dependence of the peak-to-peak potential separation (ΔE_P) between the cathodic and anodic waves as a function of the scan rate was investigated (Figure 3D). At low scan rates, ΔE_P were close to nil but nonzero, giving values of 15 and 25 mV for Cyt c and Nb, respectively. This unusual quasireversibility observed under conditions where the electron transfer is not rate limiting has been previously noticed with immobilized proteins.[32] It was notably reported for Cyt c adsorbed on different electrode materials such as ITO or gold.[18, 33] Upon increasing the scan rate, the peak-to-peak potential separation is increased, reflecting the progressive kinetic control by the rate of electron transfer to the heme centers. From the shift of the peak potentials as a function of the scan rate, the heterogeneous electron transfer rate constant k_s has been determined by fitting the resulting trumpet plots (Figure 3D) to the theoretical curves calculated from the classical Butler−Volmer equations under thin-layer conditions. Using a charge-transfer coefficient of α = 0.5, the best fits gave k_s = 12 s^{-1} and 2 s^{-1} for Cyt c and Nb, respectively. The k_s value obtained for Cyt c is very low as compared to classical carbon or metal electrodes, but very similar to the one reported by El Kasmi et al. at a planar ITO electrode,[18] and also to the one previously found by us for MP-11 adsorbed within similar GLAD ITO electrodes.[11, 12] However, the interfacial electron transfer appears much faster at GLAD ITO electrodes than at other nanostructured metal-oxide electrodes (Table 1).

As both proteins exhibit similar size and accessible heme pockets, and no change in the coordination of the iron ion associated with the electron transfer, we assume that they exhibit similar reorganization energy associated with ET. Thus, we assume that the larger k_s value reported for Cyt c may result from an optimized protein orientation toward the metal oxide surface and therefore, on average, a decreased electron transfer distance compared to a randomly oriented protein, whereas the lower k_s value reported for Nb is in line with a randomly adsorbed protein on the ITO surface which, on average, should lead to a larger electron transfer distance. This would mean that the random adsorption of Nb not only results in a distribution of microenvironment around the accessible heme pocket of Nb, which thereby explains the larger fwhm and low n_{app} values, but also leads to a distribution of distances between the heme center and the conductive surface, thus producing an apparent lower k_s value than for adsorbed Cyt c.

Denaturation. Preconditioning the ITO electrodes appears crucial to preserve the native structure of the adsorbed protein. As shown above from cross-correlation between rR and spectroelectrochemical data, the three-dimensional structures of the two hemoproteins were not significantly affected by adsorption onto the ITO electrode when the electrode was preconditioned in a buffer solution for several hours prior to protein adsorption. This preconditioning step was indeed required to prevent the denaturation of Cyt c during its adsorption within the porous film. This was evidenced by experiments conducted with "dry" (i.e., unconditioned) ITO electrodes which after immersion in a Cyt c solution (50 μM in a 10 mM Buffer solution) for 1 hour give resonance Raman spectra and electrochemical features (Figure 4) that clearly differ from those obtained at a preconditioned ITO electrode. In the rR spectrum of non-preconditioned Cyt c-ITO electrode, the high frequency ν_2, ν_3 and ν_4 core-size marker bands indicate a low spin hexacoordinated Fe^{III} ion, similar to that obtained with the rR spectrum at a preconditioned Cyt c-ITO electrode. This is consistent with the absence of Soret band shift in the UV-visible absorption spectrum obtained at the same non-preconditioned electrode (data not shown). However, below the intense ν_4 band, the rR spectrum is significantly changed. In this frequency region, spectral congestion is reported for native Cyt c because of the activation of substituent modes, porphyrin out-of-plane modes and in-plane-E_u skeletal modes attributed to protein-induced heme distortions.[34] Accordingly, the strong intensity decrease of several bands such as γ_{21}, ν_{15} , ν_{CcCd} or ν_{11} at 571, 750, 972 and 1560 cm^{-1}, respectively, most likely indicates a heme relaxation associated with protein denaturation. The resulting rR spectrum is highly

Table 1. Surface coverage and electrochemical parameters of *Horse or Bovine heart* Cyt c, MP-11 and *human* Nb adsorbed on metal oxide electrodes.

Protein	Electrode	*l* (μm)	Γ (pmol cm^{-2})	*pH*	*Buffer*	*E*° (V) vs. NHE	k_s (s^{-1})	Ref
HH Cyt c.	2D-ITO 10Ω/□		14	7.0	Phosphate	225	18	[18]
HH Cyt c.	2D-ITO 20Ω/□		8-9.5	7.0	Phosphate	198*	3.1	[19]
HH Cyt c.	3D-SnO_2	4	5500	7.0	Phosphate	255*	1	[39]
HH Cyt c.	3D-ITO	0.17	250	7.0	Phosphate	244*	1.2	[40]
BH Cyt c.	3D-ATO	ns	1500	7.0	Hepes	195	1.35	[30]
HH Cyt c.	3D-ITO	2	450	7.0	Hepes	257	12	This work
MP-11	3D-ITO	1	2850	7.0	Hepes	-164	11	[12]
Nb	3D-ITO	2	600	5.5	MES	-103	2	This work

ns: not specified, *: Standard potentials were converted to NHE.

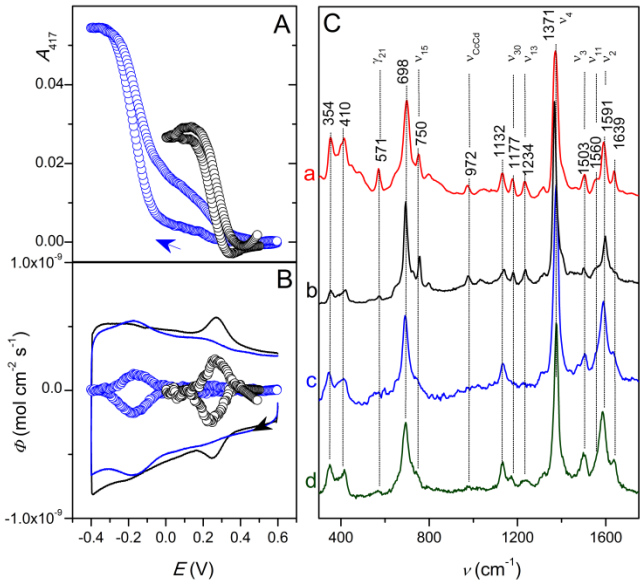

Figure 4. (A) CVAs (monitored at 417 nm) and (B) CVs concomitantly recorded at preconditioned (○, —) and non-preconditioned (○, —) Cyt c-ITO electrodes (scan rate: 50 mV s^{-1}). In B are also reported the time derivative of the CVAs shown in A. Their flux densities were calculated by using a $\Delta\varepsilon_{417}$ value of (○) 50 000 and (○) 80 000 M^{-1} cm^{-1}, respectively. (C) rR spectra (obtained under Soret excitation at λ_{exc} = 405 nm) of: (a, —) Cyt c in solution, (b, —) preconditioned Cyt c-loaded ITO electrode, (c, —) non-preconditioned Cyt c-loaded ITO electrode, (d, —) MP-11-loaded ITO electrode. All experiments were done in 90 mM Hepes, 10 mM NaCl, pH 7.0. T = 20 °C.

analogous to the one obtained for MP-11 immobilized in a GLAD ITO electrode.

When studied in cyclic voltabsorptometry, the non-preconditioned Cyt c-ITO electrode exhibits a more complex redox behavior (blue dot curve in Figure 4A), first showing a small reversible Fe^{III}/Fe^{II} absorbance change localized at 0.25 V followed by a second large reversible Fe^{III}/Fe^{II} absorbance change at -0.17 V. The comparative study between the CVA recorded at a non-preconditioned electrode (blue dot curve) and the one obtained at preconditioned electrode (black dot curve) suggests that the first reversible absorbance change corresponds to the native form of Cyt c, whereas the second one at a more negative potential appears as a denaturated form. In cyclic voltammetry the same behavior was observed, showing two separate reversible waves localized at 0.25 and -0.17 V at the non-preconditioned Cyt c-ITO electrode (blue CV curve in Figure 4B) and only one reversible wave at the preconditioned electrode (black CV curve in Figure 4B).

A more quantitative comparison between CVAs and CVs can be achieved through the conversion of CVAs (Figure 4A) into DCVAs expressed in flux densities, *ie.* using eq 1, (blue dot curve in Figure 4B). To achieve this, it is necessary to know the difference extinction coefficient of each of the different species observed on the CVAs. As a first approximation, we have used the $\Delta\varepsilon_{417}$ value reported for native Cyt c, but the resulting flux density of the DCVA was unable to match the flux density in CV (not shown). A much better correspondence was finally achieved when using, for the second reversible absorbance change, a value of $\Delta\varepsilon_{417}$ = 80 000 M^{-1} cm^{-1}, which is close to that typically obtained for MP-11, a hemoprotein with no well-defined 3D structure.[12] Accordingly,

the fraction of denaturated Cyt c was thus roughly estimated to be ~85%. It is worth noting that the relative flux density between the two DCVA reversible waves was almost unaffected by varying the scan rate (Figure S6), which indicates that the two different fraction of adsorbed Cyt c were not involved in a square reaction scheme with different conformational states.

Denaturation of Cyt c upon its adsorption on conductive surfaces has already been suggested in the literature, notably on pyrolytic graphite electrodes,[35] metallic electrodes[36] and silver electrodes modified by short-length SAM.[37] This is generally justified by a large downshift of the apparent standard potential of the Fe^{III}/Fe^{II} redox couple. Denaturation of Cyt c upon its adsorption on roughened silver electrodes was also characterized by rR spectroscopy.[36,38] Here, cross-correlation between the spectroscopic as well as spectroelectrochemical features of the non-preconditioned Cyt c-ITO electrode clearly demonstrates that the denaturated form of Cyt c is very analogous to MP-11. Similarities between both electrodes are the Soret band maximum absorbance wavelengths (406-407 nm), the rR spectra (Spectra c and d in Figure 4), the variation of extinction coefficient at 417 nm and the Fe^{III}/Fe^{II} apparent standard potentials ($E^{\circ'}_{MP-11}$ = - 164 mV).[12] Accordingly, we assume that nearly complete and irreversible Cyt c denaturation occurs during the adsorption process, leading to a solvent-exposed heme pocket and substitution of the native axial methionine ligand.

No denaturation was observed with Nb (the spectroscopic and spectroelectrochemical features of Nb-ITO electrodes were not affected by the lack of preconditioning step). This seems to be correlated to the greater stability of Nb (melting temperature of 100 °C)[41] compared to Cyt c (low temperature endotherm at 64 °C corresponding to denaturation of the heme crevice).[42] It seems also associated to the less strong interaction of Nb than Cyt c with the ITO surface. The stronger interaction of Cyt c with the negatively charged surface may indeed favor a specific protein orientation with the positively charged Lysine patch, most likely facing the conductive surface (thus optimizing the electron transfer kinetics), but at the same time it may also favor protein denaturation.[20]

CONCLUSION

We demonstrate that two small redox hemoproteins exhibiting different isoelectric points can be efficiently adsorbed within the mesostructure of a conductive transparent GLAD ITO film. This allowed their characterization by cyclic voltammetry coupled to UV-visible absorbance spectroscopy. By cross-correlation between UV-visible absorption, spectroelectrochemical data, as well as resonance Raman spectra we were able to determine the surface concentration of the adsorbed proteins and make conclusions on their conformational changes. Moreover, we performed a quantitative analysis of the thermodynamics and kinetics of the direct interfacial electron transfer between the heme and the conductive ITO surface by monitoring cyclic voltabsorptograms either in the Soret or the Q bands. Both adsorbed proteins exhibit different spectroelectrochemical features that were interpreted as arising from differences in their orientations toward the conductive ITO surface.

According to the suitably high signal-to-noise ratio obtained in resonance Raman spectroscopy, it should be interesting to couple this spectroscopy with cyclic voltammetry aiming to characterize the electron transfer processes in immobilized proteins by real-time rR spectroelectrochemistry.

EXPERIMENTAL SECTION

All chemicals, MP-11 and *Horse Heart* Cyt c were purchased from Sigma Aldrich. For GLAD ITO films, ITO-coated glass was used as the deposition substrate (8-12 Ω/□, Delta Technologies Ltd.). Experimental details concerning the film deposition are given elsewhere.[16]

The ITO electrodes were carefully rinsed with ethanol and milli-Q water before use. The geometric electrode surface was delimited to 0.3 ± 0.1 cm^2 by using nail varnish. Depending on the experiments, the ITO electrodes were preconditioned in the adsorption buffer (10 mM Hepes or MES) for ca. 12 hours prior to protein adsorption.

The spectroelectrochemical measurements were performed using a custom temperature-controlled three-electrode spectroelectrochemical cell. The reference electrode was an Ag/AgCl/KCl 3M electrode (WPI, 0.20 V *vs.* NHE) and the counter electrode a platinum wire. All potentials in the text are referred to the NHE reference. UV-visible absorption spectroscopic measurements were performed on a HR2000+ diode array spectrometer (Ocean Optics) synchronized with a potentiostat (Autolab). Cyclic voltammetric experiments were performed under ohmic drop compensation in a 1.1 mL electrolyte solution at 20 °C. The spectroelectrochemical cell was carefully degassed for 1 hour by argon bubbling prior to measurements. The integration time for spectrometric measurements was fixed at 30 ms. Depending on the time resolution required, each data point on a CVA or DCVA resulted from the averaging of 2 to 16 spectra. The DCVA was obtained from the time derivative of CVA and after applying a second order Savitsky Golay smoothing algorithm (Origin).

Resonance Raman spectra were excited at 405 nm with a single frequency collimated laser module (Ondax, Inc) and recorded with a Labram HR 800 microspectrometer (Jobin yvon). Spectra were recorded at room temperature (20 °C) with a power of 2 mW at the sample. For solution samples (20 μM protein), the microscope was equipped with an x10 objective, resulting of an excitation power of 2 mW at the sample. The reported spectra correspond to the averaging of at least 10 scans, each recorded with a 10 s acquisition time. For the measurements on GLAD ITO electrodes, the microscope was equipped with a long distance x100 objective and an optical filter (D1) to decrease the laser power on the sample to ca. 30 μW in order to avoid protein degradation. Reported spectra are the result of the average of typically 16 single spectra, each recorded with 5 s acquisition time. Measurements were performed from experiment to experiment on different surface areas to limit protein degradation.

ASSOCIATED CONTENT

Supporting Information. Complementary data on the kinetics of the adsorption process, the proteins in solution, the DCVA of denaturated Cyt c as a function of the scan rate. This material is available free of charge via the Internet at http://pubs.acs.org.

AUTHOR INFORMATION

Corresponding Author

* veronique.balland@univ-paris-diderot.fr, limoges@univ-paris-diderot.fr

Funding Sources

Financial support for DS was obtained from Agence Nationale pour la Recherche (3D-BIOELEC, ANR-11-JS08-011). Financial support for RT and MB received from NSERC, Micralyne, and Alberta Innovates: Technology Futures.

ACKNOWLEDGMENT

VB thanks Laurent Kiger (INSERM U779, Universities Paris VI and XI, Le Kremlin-Bicêtre, France) for the generous gift of *human* neuroglobin.

REFERENCES

(1) Ash, P. A.; Vincent, K. A., *Chem. Commun.* **2012,** 48, (10), 1400-1409.
(2) Murgida, D. H.; Hildebrandt, P., *Chem. Soc. Rev.* **2008,** 37, (5), 937-945.
(3) Kemp, G. L.; Marritt, S. J.; Xiaoe, L.; Durrant, J. R.; Cheesman, M. R.; Butt, J. N., *Biochem. Soc. Trans.* **2009,** 037, (2), 368-372.
(4) Ronkainen, N. J.; Halsall, H. B.; Heineman, W. R., *Chem. Soc. Rev.* **2010,** 39, (5), 1747-1763.
(5) Barton, S. C.; Gallaway, J.; Atanassov, P., *Chem. Rev.* **2004,** 104, (10), 4867-4886.
(6) Salverda, J. M.; Patil, A. V.; Mizzon, G.; Kuznetsova, S.; Zauner, G.; Akkilic, N.; Canters, G. W.; Davis, J. J.; Heering, H. A.; Aartsma, T. J., *Ang. Chem., Int. Ed.* **2010,** 49, (33), 5776-5779.
(7) Simon, A. M.; Marucci, N. E.; Saavedra, S. S., *Anal. Chem.* **2011,** 83, (14), 5762-5766.
(8) Astuti, Y.; Topoglidis, E.; Briscoe, P. B.; Fantuzzi, A.; Gilardi, G.; Durrant, J. R., *J. Am. Chem. Soc.* **2004,** 126, (25), 8001-8009.
(9) Bancroft, E. E.; Sidwell, J. S.; Blount, H. N., *Anal. Chem.* **1981,** 53, (9), 1390-1394.
(10) Marritt, S. J.; Kemp, G. L.; Xiaoe, L.; Durrant, J. R.; Cheesman, M. R.; Butt, J. N., *J. Am. Chem. Soc.* **2008,** 130, (27), 8588-8589.
(11) Renault, C.; Harris, K. D.; Brett, M. J.; Balland, V.; Limoges, B., *Chem. Commun.* **2011,** 47, (6), 1863-1865.
(12) Renault, C.; Andrieux, C. P.; Tucker, R. T.; Brett, M. J.; Balland, V.; Limoges, B., *J. Am. Chem. Soc.* **2012,** 134, (15), 6834-6845.
(13) Renault, C.; Balland, V.; Martinez-Ferrero, E.; Nicole, L.; Sanchez, C.; Limoges, B., *Chem. Commun.* **2009**, (48), 7494-7496.
(14) Robbie, K.; Friedrich, L. J.; Dew, S. K.; Smy, T.; Brett, M. J., *J. Vac. Sci. Technol., A* **1995,** 13, (3), 1032-1035.
(15) Robbie, K.; Sit, J. C.; Brett, M. J., *J. Vac. Sci. Technol., B* **1998,** 16, (3), 1115-1122.
(16) Krause, K. M.; Taschuk, M. T.; Harris, K. D.; Rider, D. A.; Wakefield, N. G.; Sit, J. C.; Buriak, J. M.; Thommes, M.; Brett, M. J., *Langmuir* **2009,** 26, (6), 4368-4376.
(17) Bowden, E. F.; Hawkridge, F. M.; Chlebowski, J. F.; Bancroft, E. E.; Thorpe, C.; Blount, H. N., *J. Am. Chem. Soc.* **1982,** 104, (26), 7641-7644.
(18) El Kasmi, A.; Leopold, M. C.; Galligan, R.; Robertson, R. T.; Saavedra, S. S.; El Kacemi, K.; Bowden, E. F., *Electrochem. Commun.* **2002,** 4, (2), 177-181.
(19) Araci, Z. O.; Runge, A. F.; Doherty, W. J.; Saavedra, S. S., *J. Am. Chem. Soc.* **2008,** 130, (5), 1572-1573.
(20) Zhou, J.; Zheng, J.; Jiang, S., *J. Phys. Chem. B* **2004,** 108, (45), 17418-17424.
(21) Hamdane, D.; Kiger, L.; Dewilde, S.; Green, B. N.; Pesce, A.; Uzan, J.; Burmester, T.; Hankeln, T.; Bolognesi, M.; Moens, L.; Marden, M. C., *Micron* **2004,** 35, (1-2), 59-62.
(22) *Theoretical pI was calculated using the ExPASy Compute pI/MW tool (http://web.expasy.org/compute_pi/)*.
(23) Balland, V.; Lecomte, S.; Limoges, B., *Langmuir* **2009,** 25, (11), 6532-6542.
(24) Kiger, L.; Tilleman, L.; Geuens, E.; Hoogewijs, D.; Lechauve, C.; Moens, L.; Dewilde, S.; Marden, M. C., *PLoS ONE* **2012,** 6, (6), e20478.
(25) Raychaudhuri, S.; Skommer, J.; Henty, K.; Birch, N.; Brittain, T., *Apoptosis* **2010,** 15, (4), 401-411.
(26) Krause, K. M.; Vick, D. W.; Malac, M.; Brett, M. J., *Langmuir* **2010,** 26, (22), 17558-17567.
(27) Sun, J.; Velamakanni, B. V.; Gerberich, W. W.; Francis, L. F., *J. Colloid Interface Sci.* **2004,** 280, (2), 387-399.
(28) Carre, A.; Roger, F. o.; Varinot, C., *J. Colloid Interface Sci.* **1992,** 154, (1), 174-183.
(29) Topoglidis, E.; Campbell, C. J.; Cass, A. E. G.; Durrant, J. R., *Langmuir* **2001,** 17, (25), 7899-7906.
(30) Kwan, P.; Schmitt, D.; Volosin, A. M.; McIntosh, C. L.; Seo, D.-K.; Jones, A. K., *Chem. Commun.* **2011,** 47, (45), 12367-12369.
(31) Spiro, T. G.; Li, X.-Y. *Biological Applications of Raman Spectroscopy*; Wiley Interscience: New York, 1988; Vol. III.
(32) Armstrong, F. A.; Camba, R.; Heering, H. A.; Hirst, J.; Jeuken, L. J. C.; Jones, A. K.; Leger, C.; McEvoy, J. P., *Farad. Disc.* **2000,** 116, 191-203.
(33) Heering, H. A.; Wiertz, F. G. M.; Dekker, C.; de Vries, S., *J. Am. Chem. Soc.* **2004,** 126, (35), 11103-11112.
(34) Hu, S.; Morris, I. K.; Singh, J. P.; Smith, K. M.; Spiro, T. G., *J. Am. Chem. Soc.* **1993,** 115, (26), 12446-12458.
(35) Ye, T.; Kaur, R.; Senguen, F. T.; Michel, L. V.; Bren, K. L.; Elliott, S. J., *J. Am. Chem. Soc.* **2008,** 130, (21), 6682-6683.
(36) Smulevich, G.; Spiro, T. G., *Journal of Physical Chemistry* **1985,** 89, (24), 5168-73.
(37) Murgida, D. H.; Hildebrandt, P., *Phys. Chem. Chem. Phys.* **2005,** 7, (22), 3773-3784.
(38) Murgida, D. H.; Hildebrandt, P., *Acc. Chem. Res.* **2004,** 37, (11), 854-861.
(39) Topoglidis, E.; Astuti, Y.; Duriaux, F.; Grätzel, M.; Durrant, J. R., *Langmuir* **2003,** 19, (17), 6894-6900.
(40) Frasca, S.; von Graberg, T.; Feng, J.-J.; Thomas, A.; Smarsly, B. M.; Weidinger, I. M.; Scheller, F. W.; Hildebrandt, P.; Wollenberger, U., *ChemCatChem* **2010,** 2, 839-845.
(41) Hamdane, D.; Kiger, L.; Dewilde, S.; Uzan, J.; Burmester, T.; Hankeln, T.; Moens, L.; Marden, M. C., *FEBS Journal* **2005,** 272, (8), 2076-2084.
(42) Muga, A.; Mantsch, H. H.; Surewicz, W. K., *Biochemistry* **1991,** 30, (29), 7219-7224.